Journal of Environmental Management 101 (2012) 1–6

Contents lists available at SciVerse ScienceDirect

Journal of Environmental Management

journal homepage: www.elsevier.com/locate/jenvman

Photocatalytic degradation of acridine dyes using anatase and rutile TiO_2

C.E. Zubieta [b,c,*], P.V. Messina [a,c], P.C. Schulz [a]

[a] Departamento de Química, Universidad Nacional del Sur e INQUISUR (CONICET), Av. Alem 1253, Bahía Blanca B8000CPB, Argentina
[b] IFISUR, Universidad Nacional del Sur, Av. Alem 1253, Bahía Blanca B8000CPB, Argentina
[c] CONICET, Av. Alem 1253, Bahía Blanca B8000CPB, Argentina

ARTICLE INFO

Article history:
Received 26 September 2011
Received in revised form
30 January 2012
Accepted 5 February 2012
Available online 2 March 2012

Keywords:
Titania
Microemulsion
Photodegradation
Pollution
Acridine dyes
Adsorption

ABSTRACT

The adsorption and photodegradation of acridine orange (AO) and acriflavine (AF) dyes on two mesoporous titania crystalline phases, anatase and rutile, were experimentally studied. Anatase and rutile were characterized by nitrogen adsorption, electron scanning and transmission microscopy, and X-ray diffraction. The adsorption capacity of rutile was higher than that of anatase, while the reverse is observed for photodegradation of both dyes. The adsorption of AF on both adsorbents was higher than that of AO, which was related with the smaller size of AF molecules compared with those of AO, therefore the access of AF to the adsorption sites is favored.

1. Introduction

Acridine orange (AO) and acriflavine (AF) dyes are members closely related to the xanthene class. Their molecular structures are shown in Fig. 1A and B respectively. Like xanthenes, they have a long history of biological applications as stains. Acridines are of inadequate stability for more demanding applications such as textile coloration (Gurr, 1960).

Acridine orange is widely used in the fields of printing and dying, leather, printing ink and lithography (Xie et al., 2000). Aminoacridines have mutagenic effects because they bind to DNA molecules and intercalate inside the double chain causing local interruptions of the unions among nitrogen bases (Ullmann, 2001). Such interruptions cause errors in the DNA replications. Acridine dyes are difficult to remove from water by conventional methods such as coagulation, chemical oxidation, precipitation, flocculation and biodegradation. The release of such effluents into the environment is a dramatic source of water pollution, eutrophication and perturbation of aquatic life (Faisal et al., 2007).

Heterogeneous photocatalysis has been successfully used in the oxidation, decontamination or mineralization of organic and inorganic contaminants in wastewater without generating harmful by products (Wong et al., 2011).

In general TiO_2 is recognized as the most efficient, nontoxic, and stable photocatalyst. Mechanistically, the photocatalyst TiO_2 is first excited by UV light and subsequently initiates the photodegradation process. The most important step of photodegradation under UV light irradiation is the production of hydroxyl radicals (Saquib et al., 2008). This radical is a powerful oxidant that can be used to degrade many organic contaminants into carbon dioxide and water (S-Amiri et al., 1996).

The unique properties of titania have found diverse applications, such as pigments (Pratsinis et al., 1996), cosmetics (Rossatto et al., 2003), catalysts (Chen and Yang, 1993), photocatalysts (Rao and Dube, 1996), etc.

Under alkaline conditions, the TiO_2 surface bears a weak negative charge, while AO and AF are in their protonated form, thus facilitating adsorption and promoting photocatalytic degradation (Chung-Shin et al., 2008). The aim of this work is to evaluate the removal (by adsorption and degradation) of acridine orange and acriflavine dyes by the utilization of commercial anatase – (Sigma–Aldrich) and rutile TiO_2 – obtained from an Aerosol OT (AOT, $C_{20}H_{37}NaO_7S$)/hexane/water reverse microemulsion. Synthesis of nanoparticles via inverse microemulsions was previously used by many authors (Yang and Gao, 2005; Addamo et al., 2008; Chung-Hsin et al., 2008). Preparation methods using extremely small water pools in reverse micelles as the reaction media have been studied extensively. One of

* Corresponding author. IFISUR, Universidad Nacional del Sur, Av. Alem 1253, Bahía Blanca B8000CPB, Argentina. Tel.: +54 291 154710377; +54 291 4595100x2815.
E-mail addresses: czubieta@uns.edu.ar, carozubieta80@hotmail.com (C.E. Zubieta).

0301-4797/$ – see front matter © 2012 Published by Elsevier Ltd.
doi:10.1016/j.jenvman.2012.02.014

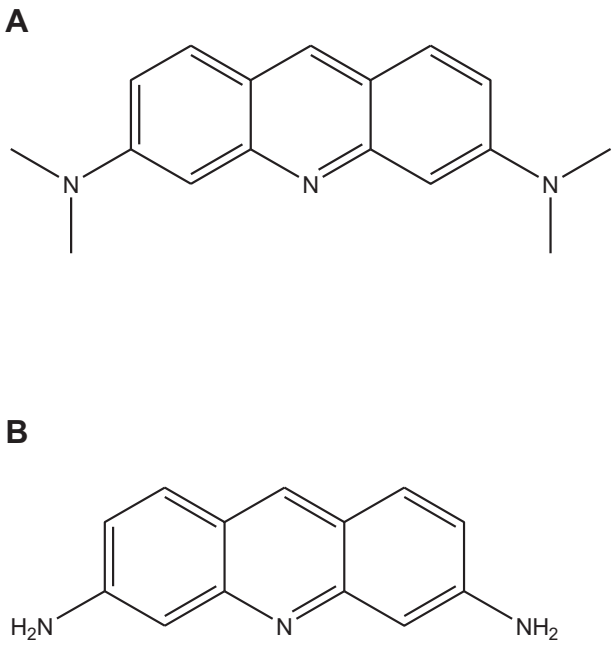

Fig. 1. Molecular structures of acridine dyes. A) AO, B) AF.

the advantages of this method is that localized supersaturation of the reactants is suppressed, and a uniform nucleation occurs, since the reactants are dispersed very well in the reverse micellar solution. In addition, the reverse micelles can protect the nanoparticles against excessive aggregation. As examples, CdS nanoparticles have been prepared in reverse micellar solutions such as AOT/isooctane or AOT/heptane systems (Messina et al., 2006).

2. Experimental

2.1. Synthesis of rutile catalysts

To obtain mesoporous titania, a reverse microemulsion solution was prepared by mixing 1.1276 g AOT in 1.5 g of water. Then the mixture was left 3 h for the surfactant hydratation be produced. We have called R (water/surfactant ratio) to the relationship of molar concentrations between the water and the surfactant (AOT) used to produce the microemulsion. In this case the water/surfactant ratio (R) was $R = 30$. Then 80 mL of n-hexane (Carlo-Erba, p.a) were added and the system was sonicated to produce the microemulsion. Then 1.4 mL of $TiCl_4$ (Carlo Erba, 99%, $\rho = 1.722$ g/cm^3) were added and left three days for the following reaction to produce:

$$2H_2O_{(l)} + TiCl_{4(l)} \rightarrow TiO_{2(s)} + 4HCl_{(g)} \quad (1)$$

The excess of HCl and n-hexane was eliminated by evaporation under vacuum. The resulting material was left 3 h in hydrothermal treatment at 70 °C in autoclave. An enhancement of crystallinity can be obtained by thermal treatment but the temperature must be carefully selected (Addamo et al., 2008; Chung-Hsin et al., 2008).

A white powder composed by the titania nanoparticles surrounded by AOT was precipitated, and was then calcinated during 7 h at 540 °C under air flux for a complete crystallization and surfactant elimination.

The materials were characterized by X-ray powder diffraction (XRD), Scanning Electron Microscopy (SEM), Transmission Electron Microscopy (TEM) and Nitrogen adsorption isotherms.

Acridine dyes were obtained from Sigma–Aldrich, and were used without any further purification. Aqueous dye solutions were prepared by using only double distilled water.

2.2. Characterization

2.2.1. X ray diffraction analysis

Powder X-ray diffraction (XRD) experiments were performed in a Philips PW 1710 difractometer with CuK_α radiation ($\lambda = 1.5418$ Å) and graphite monochromator operated at 45 kV; 30 mA and 25 °C.

2.2.2. Nitrogen adsorption isotherms

Nitrogen adsorption isotherms were measured at 77.6 K with a Micrometrics Model Accelerated Surface Area and Porosimetry System (ASAP) 2020 instrument. Each sample was degassed at 373 K for 720 min at pressure of 10^{-4} Pa.

The pore volume (Single point adsorption total pore volume of pores less than 136.6 nm width at $P/P_o = 0.9856$) and pore size (Adsorption average pore width (4V/A by BET)) were also informed.

2.2.3. Scanning electron microscopy (SEM)

Scanning electron microscopy was performed using a JEOL 35 CF. Tokio, Japan.

2.2.4. FT-IR spectroscopy

FT-IR experiments were recorded in a Nicolet FT-IR Nexus 470 Spectrophotometer.

Adsorption experiments (in darkness to avoid photodegradation) were carried out in 5 ml glass-stopped round bottom flasks immersed in a thermostatic shaker bath. For this, 50 mg of adsorbent were mixed with 5 ml of aqueous dye solutions with (0.040–0.098 mM) concentration range for AO and (0.020–0.061 mM) for AF. These concentrations were selected to ensure low error in the measurement by the UV–Vis technique. The flasks and their content were shaken at 25 °C, 35 °C and 45 °C. The stirring speed was kept constant at 90 rpm. At the end of the adsorption period, the supernatant was centrifuged for 3 min at a speed of 3500 min^{-1}. The supernatant AO and AF concentration before and after adsorption was determined using a Spectronic −20 UV–vis spectrophotometer at 449 nm and 450 nm, respectively. The adsorption time was around 700 h for both dyes.

To study the effect of the photodegradation, the same experiments were carried out in presence of UV light at $T = 25$ °C. A DESAGA UV 131000 lamp ($\lambda = 366$ nm) was applied as a radiation source for the photodegradation of dyes. Light intensity was estimated as $I_a = 2.7 \times 10^{-6}$ mol photon s^{-1} from the supplier's data. To discriminate between both effects (adsorption and photodegradation) the results of the experiments without light were subtracted from those carried out under irradiation.

Samples were made with 0.2 g of catalytic material in 10 mL of dye solution. At different irradiation times, 2 mL of the supernatant was separated and centrifuged. The change in dye concentration before and after degradation was spectrophotometrically determined at 449 nm for AO and 450 nm for AF dye.

We studied the removal (by adsorption and photodegradation) of AO and AF in a buffered solution of monobasic sodium phosphate/dibasic sodium phosphate (pH = 8.0). The formation of active $OH^\bullet$ species is favoured by this pH value, because of both, an improved transfer of holes to the adsorbed hydroxyls, and the electrostatic attractive effects, operating between the negatively charged TiO_2 particles and the operating cationic dyes (Chung-Shin et al., 2008). Similar results have been found in the photodegradation of malachite green on TiO_2 particles (Chen et al., 2007).

3. Results and discussion

3.1. Characterization of the titania materials

The XRD patterns of TiO_2 powders synthesized at water/surfactant ratio equal to $R = 30$ are displayed in Fig. 2. The composition of rutile synthesized via reverse microemulsion was determined by using the XRD patterns and the correlations given by Zhuang and Banfield (2000).

Fig. 2 shows only two peaks in $2\theta = 27^\circ$ and 35.9°, indicating that the TiO_2 adsorbent is composed only of rutile phase. The composition of anatase 99% from Sigma–Aldrich is not shown here.

Both specific surface areas and pore sizes of the samples were determined from the nitrogen adsorption data using the Brunauer–Emmet–Teller technique. Nitrogen adsorption–desorption isotherms for rutile and anatase is shown in Fig. 3. Both TiO_2 materials show the typical N_2 adsorption isotherm type IV (Sing, 1985). It is characteristic of mesoporous materials based on IUPAC classification. The *t*-plots in Fig. 4 show the appearance of the materials having slit shaped pores (Radjy and Sellevold, 1972).

SEM photomicrograph of anatase (Fig. 5A) shows that the material is formed by an agglomeration of nearly spherical particles having an average diameter of 100 nm. Analysis of the nitrogen adsorption isotherm gave the following results: $A_{BET} = 9.91\ m^2\ g^{-1}$, the mean pore radius is 10.07 nm and the mean pore volume is $0.0250\ cm^3\ g^{-1}$. The microstructure was confirmed by TEM (not shown). Analysis of the nitrogen adsorption isotherm of rutile gave the following results: BET surface area $A_{BET} = 3.83\ m^2\ g^{-1}$, mean pore radius 11.68 nm, mean pore volume $0.0112\ cm^3\ g^{-1}$. The SEM microphotographs (Fig. 5B) showed that the rutile material seems a sponge with large pores. The higher magnification obtained by TEM showed some lamellae forming slit-shaped micropores (not shown).

Pore size distribution plots of TiO_2 materials were also drawn (not shown). Following the definition of IUPAC, both materials are mesoporous (pore radius between 1 and 25 nm).

Fig. 6 shows the IR transmission spectra of anatase powder. The broad band observed at $3401\ cm^{-1}$ (O–H asymmetrical and symmetrical stretching vibrations) and the band at $1630\ cm^{-1}$ (H–OH deformation vibration) are assigned to the Ti–OH stretching modes. These bands are evidence of the presence of water molecules (Bezrodna et al., 2004). The prominent band at $\sim 580\ cm^{-1}$ corresponds to the TiO_2 lattice vibrations (Farmer, 1974).

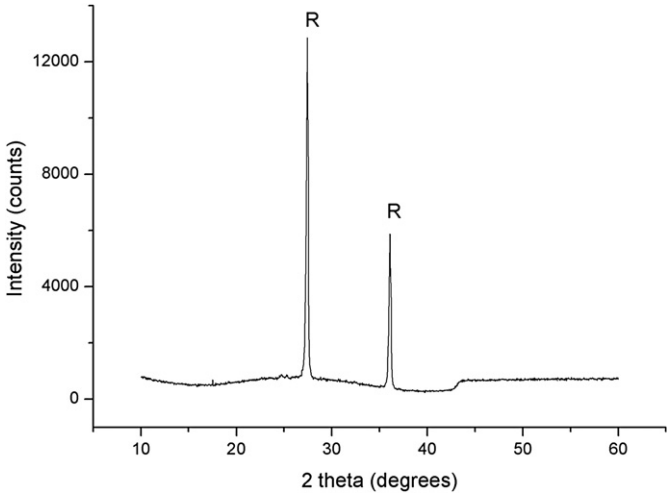

Fig. 2. The XRD patterns of TiO_2 powders synthesized at water/surfactant ratio equal to $R = 30$.

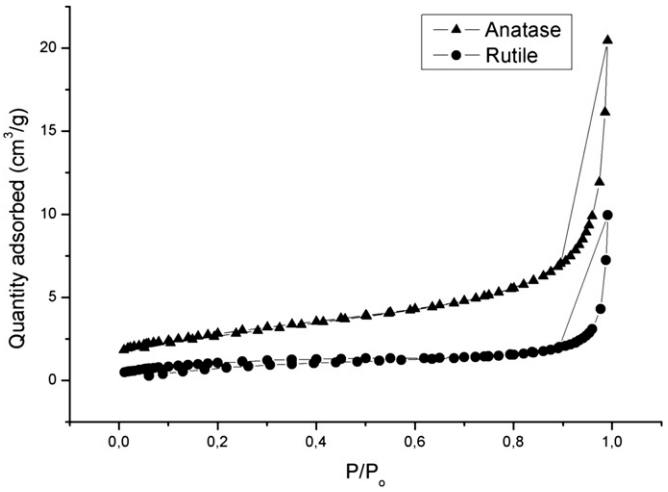

Fig. 3. The nitrogen adsorption–desorption isotherms of anatase and rutile.

3.2. Adsorption from aqueous solution

The equilibrium adsorption capacity q_e (mmol/g) of acridine dyes was calculated through the following equation:

$$q_e = \frac{(C_o - C_e)V}{m} \tag{2}$$

where C_o is the initial concentration (mmol/dm^3), C_e the residual concentration at equilibrium (mmol/dm^3), V the solution volume (dm^3), and m is the adsorbent mass (g). Two isotherm equations were used to analyze the data. One of them is the Langmuir equation, based on the hypothesis that the maximum adsorption corresponds to a saturated monolayer of adsorbate molecules on the adsorbent surface, with constant energy of interaction:

$$q_e = \frac{q_{mon} K_L C_e}{1 + K_L C_e} \tag{3}$$

where K_L is the Langmuir constant related to the energy of adsorption ($K_L = Ae^{-\Delta H/RT}$, where A is a constant, R the gas constant, T the absolute temperature and ΔH the energy of adsorption, which must be constant in the Langmuir model); and q_{mon} (mmol/g of adsorbent) is the maximum amount of adsorption corresponding to a complete coverage on the surface by a monolayer of dye.

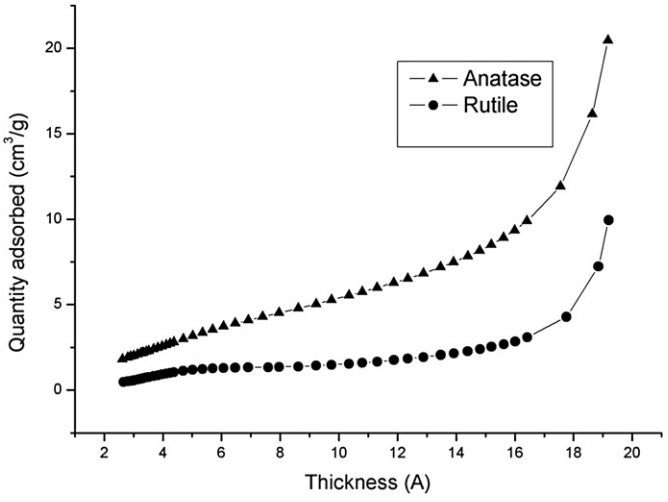

Fig. 4. The *t*-plots of anatase and rutile.

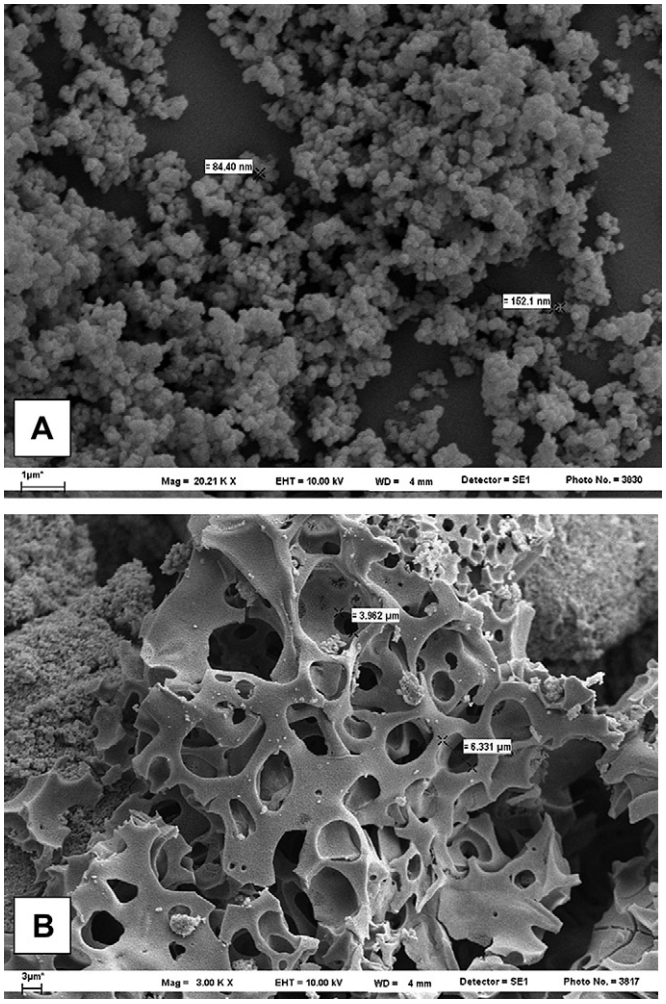

Fig. 5. The SEM microphotographs. A) anatase, B) rutile.

It must be emphasized that the theoretical interpretation of Langmuir equation parameters must be cautiously, since the fitting of experimental data to this isotherm is not a sensitive test of the model (Hiemenz and Rajagopalan, 1997).

The other model here employed is the Freundlich isotherm, which can be used for non-ideal adsorption that involves heterogeneous adsorbent surfaces (Adamson and Gast, 1997), and is expressed by the equation:

$$q_e = K_F C_e^{1/n} \quad (4)$$

where K_F is related to the adsorption capacity and $1/n$ is related to the adsorption intensity. In general, as K_F increases the adsorption capacity of an adsorbent for a given adsorbate augments. K_F can be related to the surface energy of adsorption: $K_F = RTAe^{\Delta H/RT}$, where A is a constant. The magnitude of the exponent $1/n$ gives an indication of the favorability of adsorption.

The parameters obtained from the linear fitting of adsorption data with the isotherms of Langmuir and Freundlich are presented in Table 1 for a temperature of 25 °C.

Comparing the q_{mon} values obtained from Langmuir equation the monolayer is more compact on rutile than for anatase for both dyes. It also may be noted that the amount of adsorbed AF on both adsorbents is larger than that of AO, which was related with the smaller size of AF molecules compared with those of AO, therefore the access of AF to the adsorption sites is favored. This fact can be verified by inspection of the values of q_m in Table 1.

The intensity of adsorption (given by K_L) for both dyes is very different and depends on dyes and TiO_2 surface. On anatase, the AF and AO interaction is similar. On rutile, the AO interaction is stronger than that of AF. The adsorption of acridine orange (AO) on both adsorbents is stronger than that of acriflavine (AF). This may be caused by the higher basic character of $-N(CH_3)_2$ of AO groups compared to that of $-NH_2$ of AF, which interact with the oxygen atoms on the adsorbent surface. Another possible factor was related to a bicontinuous structure of rutile with macropores with a diameter or about 6 μm (see Fig. 5B).

The value of $1/n$ for AO on anatase (1.28) is significantly higher than that on rutile (0.952) which indicates that the interaction on anatase is more favorable. The difference is not significant for AF: 0.91 on anatase, 0.99 on rutile.

Taking into account the specific area of both adsorbents (9.92 $m^2 g^{-1}$ for anatase, 3.83 $m^2 g^{-1}$ for rutile), the area occupied per dye molecule on the TiO_2 materials at 25 °C on anatase is $a_{mon} = 71.5$ Å^2/molecule for AF and $a_{mon} = 91.8$ Å^2/molecule for AO. On rutile, $a_{mon} = 2$ Å^2/molecule for AF and $a_{mon} = 5$ Å^2/molecule for AO.

The fitting of the experimental data on rutile is better for Freundlich equation than for that of Langmuir, which supports the interpretation that the adsorbent/dye interface is heterogeneous, while in anatase there is no significant difference between both isotherms, suggesting that the adsorbent interface is probably homogeneous. There is no assurance that the derivation of the Freundlich equation is unique; consequently, if the data fit the equation, it is only likely, but not proved, that the surface is heterogeneous (Adamson and Gast, 1998). Since in many cases the Langmuir equation gives adequate results in systems in which surface heterogeneity is known to be present (Hiemenz and Rajagopalan, 1997), the fitting of the data by both models with similar correlation coefficients is possible.

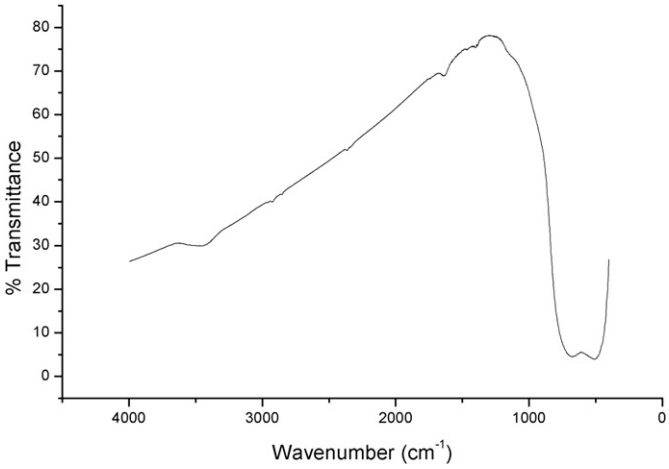

Fig. 6. The IR transmission spectra of anatase powder.

Table 1
Adsorption parameters of the tested acridine dyes on rutile and anatase TiO_2, being r^2 the correlation determination.

Dye	TiO_2	Langmuir			Freundlich			
		q_{mon} (mmol/g)	K_L (L/mmol)	r^2	n	$1/n$	K_F	r^2
AO	Anatase	0.0179	3.41	0.89	0.783	1.28	0.0981	0.98
AO	Rutile	0.127	0.569	0.99	1.05	0.95	0.0614	0.99
AF	Anatase	0.0230	3.76	0.99	1.10	0.91	0.057	0.99
AF	Rutile	0.319	0.196	0.99	1.01	0.99	0.0598	0.99

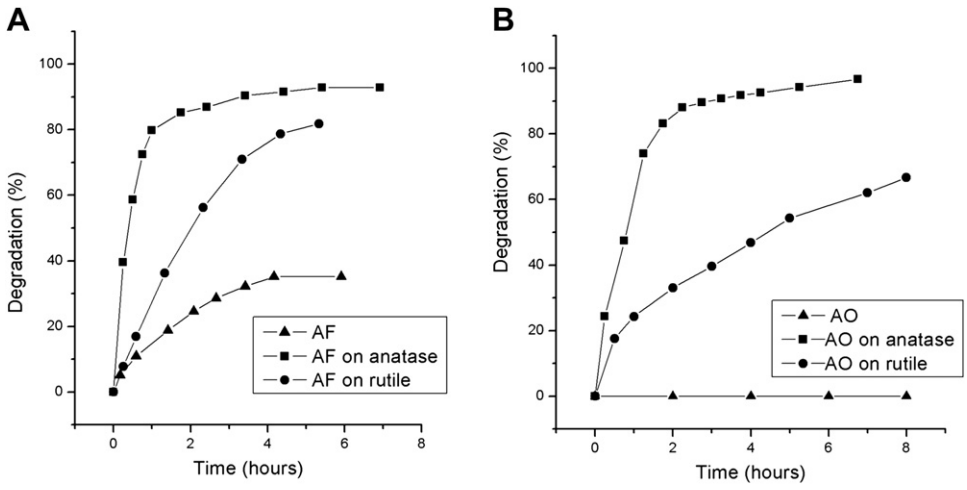

Fig. 7. The photodegradation of acridine dyes on anatase and rutile. A) AF, B) AO.

3.3. Photocatalytic activity

The photocatalytic activity of both anatase and rutile particles was investigated using aqueous solutions of AF (0.061 mM) and AO (0.096 mM). The photocatalytic activity was evaluated as the percentage of pollutant disappearance.

Fig. 7A shows the photodegradation of AF on anatase and rutile. In this case irradiation without catalyst produced a degradation of 35%. With anatase the degradation was 93% in about 5.4 h, while with rutile it was 82% in 5.3 h. Fig. 7B shows the results for AO. With no catalyst there was not degradation. The maximum degradation was 97% reached in 6.7 h on anatase and 67% in 8 h on rutile.

The degradation rate was monitored by studying the contact time throughout exposition to UV. Pseudo first -order and pseudo second-order kinetic models were tested in this study in which the experimental data obtained for various contact time were used.

The pseudo first-order equation is

$$\ln(q_e - q_t) = \ln q_e - k_1 t \quad (5)$$

where k_1 is the pseudo-first order rate constant (h^{-1}).

The pseudo second-order equation is

$$\frac{t}{q_t} = \frac{1}{k_2 q_e^2} + \frac{1}{q_e} t \quad (6)$$

where k_2 is the pseudo-second order rate constant ($mmol^{-1}\,gh^{-1}$).

Results show that the second-order kinetic model fits perfectly the experimental data, with linear regression coefficients greater than 0.98. Photocatalytic efficiency (%) and kinetic parameters of the titania samples towards acridine dyes photodegradation are displayed in Table 2.

The results of photocatalysis experiments confirmed that degradation of acridine dyes is slower with the rutile sample compared to the anatase sample. A higher photocatalytic activity of anatase may be due to surface porosity, band width and the presence of hydroxyl groups (Tayade et al., 2007). The specific area on anatase was larger than that of rutile (9.91 m^2/g and 3.83 m^2/g, respectively). A larger specific surface gives a larger amount of active sites and lower recombination of holes and electrons, which is the step determining the rate of photodegradation. The photocatalytic process is highly dependent on the hydroxyl group present on the surface, which is in turn related to the specific area. Besides, the optimal band width is another important factor in the photocatalytic activity (Tayade et al., 2007). For anatase the band width is 3.2 eV, whereas that of rutile is 3.0 eV, and this makes the recombination of the electron–hole pairs more difficult in anatase.

Table 2
Photocatalytic efficiency (%) and kinetic parameters of the titania samples towards acridine dyes photodegradation.

Dye on TiO_2	Degradation (%)	Time to complete degradation (h)	Photodegradation rate constants ($mmol^{-1}gh^{-1}$)	r^2
AO on anatase	97	6.7	132.3	0.99
AO on rutile	67	8.0	51.9	0.98
AF on anatase	93	5.4	742	0.99
AF on rutile	82	5.3	215.5	0.99

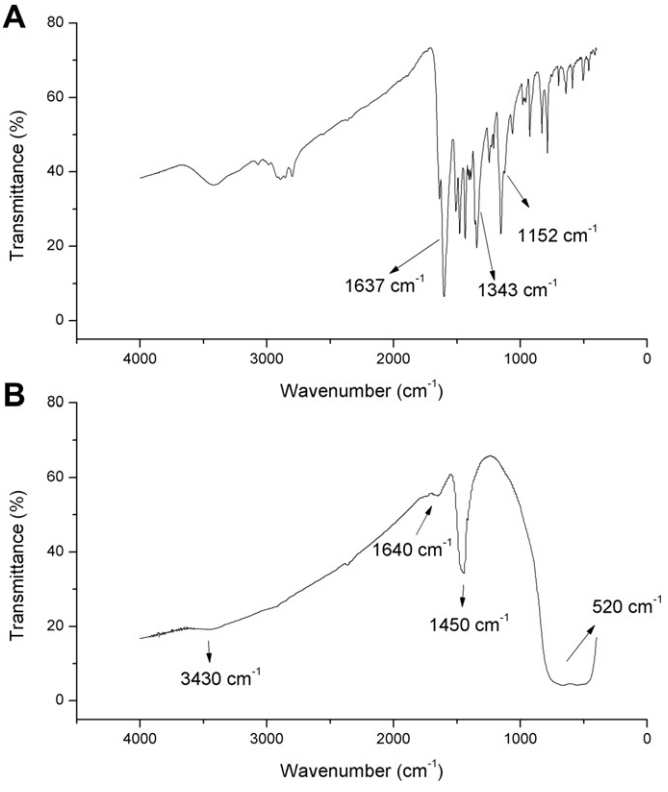

Fig. 8. A) The FT-IR spectrum of AO dye, B) The FT-IR spectrum of anatase TiO_2 at the end of the photodegradation process.

Degradation rate constants of acridine dyes for both anatase and rutile from Table 2 clearly show that the degradation of AF is faster than that in AO one in both TiO_2 materials. At this stage of our knowledge, we cannot explain this difference. This may be the subject of further research.

The FT-IR of both AO dye before UV irradiation treatment, and anatase sample at the end of the photodegradation process are shown in Fig. 8A and B, respectively.

According to the IR spectrum of the AO sample (Fig. 8A), the absorption peaks at 1637, 1343 and 1152 cm^{-1} are due to the stretching vibrations of the frame of the conjugated ring, the stretching vibrations of Ar–N bonds and the bending vibrations of Ar–H bonds, respectively. From Fig. 8B, we can also infer that the characteristic peaks apparently changed at the end of the degradation period. We noticed the prominent band in 520 cm^{-1} and the broad band in 3430 cm^{-1} which are attributable to the TiO_2 lattice vibrations and water molecules respectively. However, two bands appeared: an intense band in 1450 cm^{-1} and another smaller one in 1640 cm^{-1}. The band around 1450 cm^{-1} could be assigned to N–H deformation vibration of NH_4^+ monomer (Scheinmann, 1970; Datka et al., 1995). The second band, probably could be attributed to ammonia hydrogen-bonded with Ti–OH groups as well as ammonia hydrogen bonded was found with non-acidic silanol groups (Micek-Ilnicka et al., 2005).

Similar results were found from the photodegradation of AO on rutile catalyst and AF on both surfaces (not shown here).

4. Concluding remarks

Rutile TiO_2 has been prepared by microemulsion route. Commercial anatase was provided by Sigma–Aldrich. Both materials were characterized by different techniques. Anatase and rutile TiO_2 were mesoporous with 9.91 m^2/g and 3.83 m^2/g respectively. The adsorption and photocatalytic activity of both materials was investigated.

Experimental results indicate that the adsorption capacity of rutile is higher than that of anatase, despite the higher specific area of the latter. Data also suggest that the adsorption surface of rutile is heterogeneous. The adsorption of acridine orange (AO) on both adsorbents is stronger than that of acriflavine (AF). This may be caused by the higher basic character of $-N(CH_3)_2$ of AO groups compared to that of $-NH_2$ of AF, which interact with the oxygen atoms on the adsorbent surface. Another possible factor was related to a bicontinuous structure of rutile with macropores with a diameter or about 6 μm.

Kinetic results confirm that degradation of acridine dyes in the rutile sample is slower than the one in the anatase sample.

The results of photocatalysis experiments confirmed that degradation of acridine dyes in the rutile sample is slower than the one in the anatase sample. The degradation rate constants of acridine dyes for both anatase and rutile, clearly show that the degradation of AF is faster than that of AO in both TiO_2 materials. According to the IR study of dyes and materials after the photodegradation period, we can infer that the dye molecules were oxidized by TiO_2 materials into water and the corresponding mineralized products (CO_2 and NH_4^+).

Acknowledgements

This work was supported by a grant from the Universidad Nacional del Sur and another from Agencia Nacional de Promoción Científica y Tecnológica de la República Argentina (ANPCyT). PM is an adjunct researcher and CZ has a grant from the Consejo Nacional de Investigaciones Científicas y Técnicas de la República Argentina (CONICET).

References

Adamson, A.W., Gast, A.P., 1997. Physical Chemistry of Surfaces, sixth ed. Wiley, New York, pp. 336–338.
Adamson, A.W., Gast, A.P., 1998. Physical Chemistry of Surfaces, sixth ed. Wiley, New York, pp. 393–394.
Addamo, M., Bellardita, M., Carriazo, D., Di Paola, A., Milioto, S., Palmisano, L., Rives, V., 2008. Inorganic gels as precursors of TiO_2 photocatalysts prepared by low temperature microwave or thermal treatment. Applied Catalysis B: Environmental 84, 742–748.
Bezrodna, T., Puchkovska, G., Shymanosvska, V., Baran, J., Ratajczak, H., 2004. IR-analysis of H-bonded H2O on the pure TiO_2 surface. Journal of Molecular Structure 700, 175–181. and references therein.
Chen, C.C., Lu, C.S., Chung, Y.C., Jan, J.L., 2007. UV light induced photodegradation of malachite green on TiO_2 nanoparticles. Journal of Hazardous Materials 141, 520–528.
Chen, J.P., Yang, R.T., 1993. Selective catalytic reduction of NO with NH_3 on SO_4^{2-}/TiO_2 superacid catalyst. Journal of Catalysis 139, 277–288.
Chung-Hsin, L., Wei-Hong, W., Rohidas, B.K., 2008. Microemulsion-mediated hydrothermal synthesis of photocatalytic TiO_2 powders. Journal of Hazardous Materials 154, 649–654.
Chung-Shin, L., Fu-Der, M., Chia-Wei, W., Ren-Jang, W., Chiing-Chang, C., 2008. Titanium dioxide-mediated photocatalytic degradation of Acridine Orange in aqueous suspensions under UV irradiation. Dyes and Pigments 76, 706–713.
Datka, J., Gil, B., Kubacka, A., 1995. Acid properties of NaH-mordenites: infrared spectroscopic studies of ammonia sorption. Zeolites 15, 501–506.
Faisal, M., Tariq, M.A., Muneer, M., 2007. Photocatalysed degradation of two selected dyes in UV irradiated aqueous suspensions of titania. Dyes and Pigments 72, 233–239.
Farmer, V.C., 1974. In: Farmer (Ed.), The Infrared Spectra of Minerals. V.C. Mineral Society, London.
Gurr, E., 1960. Encyclopedia of Microscopic Stains. Leonard Hall, London. 367–377.
Hiemenz, P.C., Rajagopalan, R., 1997. Principles of Colloid and Surface Chemistry, third ed. Dekker, New York, pp. 336–338.
Messina, P., Morini, M., Sierra, M.B., Schulz, P.C., 2006. Mesoporous silica–titania composed materials. Journal of Colloids and Interface Science 300, 270–278. and reference therein.
Micek-Ilnicka, A., Gil, B., Lalik, E., 2005. Ammonia sorption by Dawson acid studied by IR spectroscopy and microbalance. Journal of Molecular Structure 740, 25–29.
Pratsinis, S.E., Zhu, W., Vemury, S., 1996. The role of gas mixing in flame synthesis of titania powders. Powder Technology 86, 87–93.
Radjy, F., Sellevold, E., 1972. A phenomenological theory for the t-method of pore structure analysis: I. Slit-shaped pores. Journal of Colloids and Interface Science 39, 367–388.
Rao, N.N., Dube, D., 1996. Photocatalytic degradation of mixed surfactants and some commercial soap/detergent products using suspended TiO_2 catalyst. Journal of Molecular Catalysis A Chemistry 104, 197–199.
Rossatto, V., Picatonotto, T., Vione, D., Carlotti, M.E., 2003. Behaviour of some rheological modifiers used in cosmetics under photocatalytic conditions. Journal of Dispersion Science and Technology 24, 259–271.
S-Amiri, A., Bolton, J.R., Cater, S.R., 1996. Ferrioxalate-mediated solar degradation of organic contaminants in water. Solar Energy 56, 439–443.
Saquib, M., Abu Tariq, M., Haque, M.M., Muneer, M., 2008. Photocatalytic degradation of disperse blue 1 using $UV/TiO_2/H_2O_2$ process. Journal of Environmental Management 88, 300–306.
Scheinmann, F., 1970. An Introduction to Spectroscopic Methods for the Identification of Organic Compounds, vol. 1. Pergamon Press, New York, p. 185.
Sing, K.S.W., 1985. Reporting physisorption data for gas/solid Systems with special reference to the determination of surface area and porosity. Pure & Applied Chemistry 57, 603–619.
Tayade, R.J., Surolia, P.K., Kulkarni, R.G., Jasra, R.V., 2007. Photocatalytic degradation of dyes and organic contaminants in water using nanocrystalline anatase and rutile TiO_2. Science and Technology of Advanced Materials 8, 455–462.
Ullmann, F., 2001. Triarylmethane and Diarylmethane Dyes. Ullmann's Encyclopedia of Industrial Chemistry, sixth ed. Wiley-VCH, New York. A. 27.
Wong, C.L., Tan, Y.N., Mohamed, A.R., 2011. A review on the formation of titania nanotube photocatalysts by hydrothermal treatment. Journal of Environmental Management 92, 1669–1680.
Xie, Y., Chen, F., He, J., Zhao, J., Wang, H., 2000. Photoassisted degradation of dyes in the presence of Fe^{3+} and H_2O_2 under visible irradiation. Journal of Photochemistry and Photobiology A: Chemistry 136, 235–240.
Yang, S., Gao, L., 2005. Preparation of titanium dioxide nanocrystallites with high photocatalytic activities. Journal of the American Ceramic Society 88, 968–970.
Zhuang, H., Banfield, J.F., 2000. Understanding polymorphic phase transformation behaviour during growth of nanocrystalline aggregates: Insights from TiO_2. Journal of Physical Chemistry B, 3481–3487.